Chatter, process damping, and chip segmentation in turning: a signal processing approach

Christopher M Taylor[a], Sam Turner[b], Neil D Sims[a,*]

[a] *Department of Mechanical Engineering, The University of Sheffield, Mappin Street, Sheffield, S1 3JD, UK*
[b] *Advanced Manufacturing Research Center with Boeing, The University of Sheffield, Advanced Manufacturing Park, Wallis Way, Catcliffe, Rotherham S10 1GZ, UK*

Abstract

An increasing number of aerospace components are manufactured from titanium and nickel alloys that are difficult to machine due to their thermal and mechanical properties. This limits the metal removal rates that can be achieved from the production process. However, under these machining conditions the phenomenon of process damping can be exploited to help avoid self-excited vibrations known as regenerative chatter. This means that greater widths of cut can be taken so as to increase the metal removal rate, and hence offset the cutting speed restrictions that are imposed by the thermo-mechanical properties of the material. However, there is little or no consensus as to the underlying mechanisms that cause process damping.

The present study investigates two process damping mechanisms that have previously been proposed in the machining literature: the tool flank / workpiece interference effect, and the short regenerative effect. A signal processing procedure is employed to identify flank / workpiece interference from experimental data. Meanwhile, the short regenerative model is solved using a new frequency domain approach that yields additional insight into its stabilising effect. However, analysis and signal processing of the experimentally obtained data reveals that neither of these models can fully explain the increases in stability that are observed in practice. Meanwhile, chip segmentation effects were observed in a number of measurements, and it is suggested that segmentation could play an important role in the process-damped chatter stability of these materials.

Key words: turning chatter, process damping, chip segmentation, Hilbert transform

1. Introduction

During machining, undesirable vibrations between the tool and workpiece can lead to an unacceptable surface finish. Perhaps the most troublesome cause of such vibrations is regenerative chatter, where unstable self-excited oscillations lead to a wavy surface finish that can result in tool wear, tool failure, or damage to the machine. Consequently there has been a great deal of research aimed at predicting and avoiding regenerative chatter, so as to enhance the productivity of turning, milling, and other metal machining operations.

For many materials that are 'easy to machine', this research activity has helped to motivate the development of high-speed machining, where very high material rates can be combined with good chatter stability and a high quality surface finish. This approach is commonplace for the machining of aluminium alloys [1].

However, more exotic materials such as titanium and nickel alloys are being used in high-technology applications. Examples include aero-engines components (where high temperatures are found during service) and other critical aircraft structures such as landing gear. The thermal properties of these materials make tool wear a governing factor in the choice of machining process parameters. As a result, machining at high surface and spindle speeds is normally not possible [2], and the manufacturing engineer must accept the lower productivity associated with lower speeds.

At low spindle and surface speeds, the phenomenon of process damping acts to increase the stability of regenerative chatter [3]. Whilst this phenomenon has been widely debated in the literature (e.g. [4, 5, 6]), there is no consensus as to the full physical mechanisms that lead to increased stability. Nevertheless, this increased stability allows greater widths of cut to be taken, so that higher metal removal rates can be achieved. Meanwhile, process damping has become a focus of attention in various academic studies [7].

A further complication with the machining of exotic alloys is the issue of chip segmentation, where serrated chips with a saw-tooth pattern are formed as workpiece material is

*Corresponding author
Email addresses: n.sims@sheffield.ac.uk (Neil D Sims)
URL: www.dynamics.group.shef.ac.uk/people/neil (Neil D Sims)

removed [8]. This segmentation behaviour can lead to high amplitudes of forced vibration, which can be detrimental to the tool life and workpiece surface finish.

The present contribution aims to shed light on the phenomenon of process damping when machine turning a difficult-to-cut-material that forms segmented chips. This will be acheived using a signal processing approach and a frequency domain analysis. Two process damping mechanisms that have been proposed in the literature will be investigated: the 'short regenerative effect' proposed by Stépán [9, 10], and the 'flank interference concept' described by Tlusty [1, 3]. A frequency domain solution to Stepan's model will be developed, which provides additional insight into the stability improvements that are predicted. Meanwhile, a signal processing procedure is developed to interpret the vibration measurements recorded during machining, which are plagued by measurement noise and the influence of non-deterministic and unmodelled disturbances. The signal processing procedure is used to demonstrate the extent to which the process damping mechanisms can explain the vibrations that occur in practice.

The remainder of this manuscript is organised as follows. First, the theory of regenerative chatter in turning is summarised and a chatter stability model is developed in the frequency domain. The flank interference concept is then illustrated schematically. Next, the short regenerative effect proposed by Stépán is solved in the frequency domain, so that it can be incorporated into the chatter stability prediction. An experimental setup is then described whereby vibration during turning of titanium alloy can be measured. A signal processing approach is then described that aims to measure the degree of flank interference from experimental data, and characterise the vibrations obtained in practice. Analysis and discussion of the experimental data leads to conclusions regarding the relevance of chip segmentation, flank interference, and the short regenerative delay on machining of exotic alloys.

2. Theory

2.1. Regenerative chatter in turning

The concept of regenerative chatter in turning can be found in various undergraduate textbooks [1, 11], but the present study will require a slightly different approach to stability

analysis based directly on the gain and phase margins of the open loop bode diagram. For completeness, the basic stability model is therefore described.

Consider the schematic representation of turning shown in Fig. 1a. Here, the turning tool is cutting a workpiece that had a wavy surface left behind by the previous tool revolution. The time period of the workpiece revolution is T seconds, and the vibration of the workpiece surface is denoted $y(t)$. The feed rate of the tool relative to the workpiece results in a mean chip thickness h_0, which is constant. Removal of the chip by the cutting tool results in a cutting force $f_{cut}(t)$ exerted upon the tool. This cutting force results in a vibration of the tool relative to the workpiece: in the schematic representation of Fig. 1a, this vibration arises due to a single degree of freedom. The component of the cutting force acting in the direction of this degree of freedom is $-f(t)$, and this force gives rise to the relative vibration $y(t)$. It is common to assume that the component of $f(t)$ of the cutting force $f_{cut}(t)$ is given by

$$f(t) = K_n b h(t) \tag{1}$$

where b is the width of cut (into the page in Fig. 1a), and $h(t)$ is the instantaneous chip thickness:

$$h(t) = h_0 + y(t) - y(t - T) \tag{2}$$

The resulting feedback between vibration y, delayed vibration $y(t - T)$, chip thickness $h(t)$, and force $f(t)$ is the mechanism that leads to self excited vibration and regenerative chatter. This mechanism can be shown in block diagram form, as illustrated in Fig. 2. Here, the choice of coordinate systems has resulted in a negative feedback system, and the transfer function $G_{chip}(s)$ is unity. The block diagram is represented in the Laplace domain, so that the delayed vibration $y(t - T)$ is obtained from a transfer function term e^{-sT}. This delayed vibration is often referred to as the outer modulation, since it represents the vibration of the outer surface shown in Fig. 1. The flexible structure $G_s(s)$ is then excited in the y direction by the negative feedback of the cutting force. In practice, structural excitation also arises due to the presence of a disturbance force. One such force is the component of the chip segmentation force that could be considered independent of the chip thickness.

The stability of the feedback system shown in Fig. 2 can be determined by setting h_0 to zero, since it is a constant disturbance signal. The standard approach is to apply the Nyquist stability criterion and solve to find the value of b at the stability boundary, as a function of the spindle speed $\frac{60}{T}$, cutting stiffness K_n and structural dynamics $G(s)$. This value is referred to as the critical width of cut, b_{lim}. In the present study, this approach will be replaced by an analysis of the gain and phase margins for the system. This technique will now be summarised and illustrated.

Returning to Fig. 2, it can be seen that the open loop transfer function for this unity negative feedback system is:

$$G_{open}(s) = G_s(s)\left(1 - e^{-sT}\right) G_{chip}(s) K_n b \tag{3}$$

where $G_{chip}(s)$ is unity. Application of the Nyquist stability criterion for the corresponding closed loop system gives $G_{open} = -1$ at the boundary of stability. Replacing s with $j\omega$ leads to a frequency domain representation of the system. The normal definition of the gain margin for the closed loop system can then be applied: the amount of additional gain that the open loop system could tolerate before its gain becomes 0 dB when its phase response is $-180°$. Since the parameter b is simply a gain term in the open loop transfer function, setting $b = 1$ leads to a gain margin which (in non decibel form) is simply the reciprocal of b_{lim}.

This approach is illustrated with a numerical example in Fig. 3, for arbitrary values of $G_s(s)$, K_n, and T. The response of the structure $G_s(j\omega) \equiv G(s)$ has been scaled by a factor K_n, and this appears as a single degree of freedom response on the dB gain (Fig. 3a) and phase ((Fig. 3b) diagrams. Meanwhile, the regenerative term $\left(1 - e^{-sT}\right)$ has a magnitude between 0 and 2 ($-\infty$ and 6 dB), and a phase response that varies linearly from $+90°$ to $-90°$ (hence the choice of a linear frequency axis).

The total response of the open loop system can be seen to vary drastically in magnitude, whilst the phase can only approach $-180°$ in the vicinity of the natural frequency of the flexible structure. The repeating nature of the regenerative term leads to an infinite number of critical frequencies where the phase is $-180°$. However, frequencies close to a resonant

frequency of the structure G_s will have the highest magnitude. The critical frequency with the highest magnitude is the resulting chatter frequency of the system, i.e. the frequency at which unstable vibrations will start to arise. Meanwhile, the corresponding gain margin is the reciprocal of the critical width of cut b_{lim}.

This process can be repeated for a range of spindle speeds $\frac{60}{T}$ (rev/min), to determine the critical width of cut as a function of spindle speed. The result is the so-called stability lobe diagram illustrated in Fig. 3c. Here, the traditional solution [1] gives rise to repeating sequences of 'lobes', from which the lowest value (shown in bold) is chosen to give the critical width of cut. The gain margin approach gives the same candidate solutions for a predetermined spindle speed, as shown by the markers.

At this stage it is worth re-iterating the practical significance of Fig. 3c. Close inspection reveals that that size of each lobe increases slightly as the spindle speed is increased. As a result, high speed machining (where the spindle speed is 20000 rev/min or even greater in milling) can be chatter-free even at high widths of cut. This results in very high metal removal rates, and hence high productivity, for easy-to-machine materials such as aluminium alloys [1]. Meanwhile, difficult-to-machine materials such as titanium alloys require low spindle speeds [2], where the stability lobes appear to converge towards a lower value. However, it transpires that the process damping phenomenon reduces the validity of this stability analysis at low spindle speeds. Two potential process damping mechanisms will now be introduced.

2.2. Flank interference

One of the first plausible explanations of the observed increased stability at low surface speeds is summarised by Tlusty [1, 3]. When the spindle speed is low compared to the frequency of chatter vibrations, then the number of waves per revolution of the workpiece becomes higher. With reference to Fig. 1a, the waves have a shorter wavelength, as illustrated by the close-up of the tool tip shown in Fig. 1b. Here, the vibration wavelength has become so short that even for a small amplitude of vibration, the just-cut surface starts to contact with the relief face of the tool. This contact results in additional forces on the tool

which act out of phase with the velocity $\dot{y}(t)$ of the vibrations. The result is a damping phenomenon that acts to increase the stability of the system.

This is a rather conceptual explanation, since in reality the mechanics of chip removal, ploughing, and sliding contact are extremely complex. Nevertheless, it is useful to explore whether this flank interference does occur during process damped cutting. The present contribution aims to achieve this through a signal processing procedure that will be applied to experimental testing of a flexible turning system.

However, before describing the experimental activity, an alternative explanation of process damping will be reviewed and a new and insightful solution approach employed to illustrate the resulting stability.

2.3. The short regenerative effect

The short regenerative effect was first proposed by Stépán in his theoretical analysis of retarded dynamical systems [9]. More recently, the relevance of process damping to exotic materials has sparked a renewed interest in the concept (e.g. [10, 12]). With reference to Fig. 1c, the contact between the chip and the tool can be seen to be distributed along the rake face of the tool along a contact length L_c. It is reasonable to assume that the pressure distribution across this contact (and the resulting cutting force) is a function of the instantaneous chip thickness of the chip in contact with the rake face, and not the chip at the tool tip. This assumption leads to an additional delay term $G_{chip}(s)$ in the block diagram of Fig. 2. Stépán [9] proposed a weighting function to represent the relationship between this short-time-delayed chip thickness and the resulting cutting force:

$$f_y(t) = bK_n \int_0^{\tau_c} w(\tau) h(t-\tau) d\tau \tag{4}$$

Here, τ is the short time delay, and τ_c represents the time taken for the chip to pass along the contact length L_c. $w(\tau)$ is a weighting function which is chosen so that:

$$\int_0^{\tau_c} w(\tau) d\tau = 1 \tag{5}$$

Consequently the value of the cutting force coefficient K_n is unaffected. Stépán assumed various weighting functions and developed analytical solutions based upon third order retarded

differential-difference equations. This approach required a single degree of freedom flexible structure. More recently, Khasawneh *et al* [12] developed a time-finite-element solution to this class of problems, that could be extended to multiple degree of freedom flexible structures. The aim of the present section is to demonstrate a frequency domain solution that avoids any restrictions on the number of degrees of freedom of the system, whilst offering additional insight into the stability improvements that are to be gained. Begin by taking Laplace transforms of Eq. (4):

$$F_y(s) = bK_n \int_0^{\infty} \left(\int_0^{\tau_c} w(\tau) h_0(t-\tau) h(t-\tau) d\tau \right) e^{-ts} dt \tag{6}$$

where $h_0(t-\tau)$ is the Heaviside step function, which ensures that the input function to the Laplace transform has a positive real time domain. Changing the order of the integrations gives:

$$F_y(s) = bK_n \int_{\tau=0}^{\tau_c} \left(w(\tau) \int_{t=0}^{\infty} h_0(t-\tau) h(t-\tau) e^{-ts} dt \right) d\tau \tag{7}$$

Applying the time shifting property of the Laplace transform gives

$$F_y(s) = bK_n \int_{\tau=0}^{\tau_c} w(\tau) e^{-\tau s} H(s) d\tau \tag{8}$$

where $H(s)$ is not a function of τ. This gives:

$$F_y(s) = bK_n H(s) \int_{\tau=0}^{\tau_c} w(\tau) e^{-\tau s} d\tau \tag{9}$$

So for the exponential weighting function

$$w(\tau) = \frac{a}{\tau_c (1 - e^{-a})} e^{\frac{-a\tau}{\tau_c}} \tag{10}$$

the transfer function between the instantaneous chip thickness and cutting force is:

$$G_{chip}(s) = \frac{F_y(s)}{bK_n H(s)} = \left(\frac{a}{e^a - 1} \right) \left(\frac{1}{a + s\tau_c} \right) \left(e^a - e^{-s\tau_c} \right) \tag{11}$$

At this point it is useful to discuss the practical implications of the weighting function $w(\tau)$ and contact time τ. With reference to Fig. 1, the component of the cutting force f_{cut} that acts normal to the workpiece surface is primarily a result of the shear stress on the rake

face of the tool. If the rake angle of the tool is non-zero, then the normal stress will also result in a force component acting in the negative y direction. The short regenerative model assumes that the stress at some point L along the distance L_c is the value of the underlying stress distribution w modulated by the instantaneous chip thickness at that point on the rake face.

The velocity of the chip along the rake face is not necessarily the same as the surface speed (i.e. the tool velocity relative to the surface). During chip formation, the angle of the primary shear plane leads to compression of the chip before it travels up the rake face [13]. Consequently, the chip velocity is reduced by the chip compression ratio λ, and the total chip contact time τ_c depends upon the chip contact length L_c, the surface speed v_s (m/min), and the chip compression ratio λ:

$$\tau_c = \frac{60\lambda}{v_s} L_c \tag{12}$$

Recently, Iqbal *et al* [14] measured the contact length and the compression ratio of Ti6Al4V alloy, and obtained contact lengths that were generally less than 1mm and chip compression ratios that were generally less than 2. Based upon their data, a value of $\lambda L_c = 0.002$ m is a conservative upper limit for this material.

Despite this useful knowledge of the chip contact time, the nature of the stress distribution on the rake face of the tool remains unknown. Childs [13] highlights the difficulties of experimentally measuring this stress distribution using 'split tool' tests. Some example stress distributions are presented that range from exponential decays in the form of Eq. (10) to more constant distributions.

Clearly this model involves many assumptions regarding the form of the stress distribution and its relationship with the short-delayed chip thickness. The present contribution does not intend to investigate these assumptions in any detail. Instead, a variety of weighting functions are considered in the frequency domain so that their influence on chatter stability can be visualised. The resulting stability lobes will then be compared to experimental data, to investigate whether they can predict realistic stability increases, given the assumed value for λL_c. A selection of candidate weighting functions (including the exponential example

above), and the resulting transfer functions are given in Table 1.

The resulting bode diagrams are shown in Fig. 4. Note that in all of the expressions in Table 1 the bode diagram can be presented as a function of $s\tau_c$, where $s \equiv j\omega$. A clear pattern emerges for all of these weighting functions. First, the global behaviour is dominated by that of a low pass filter, where the filter bandwidth is close to $\frac{1}{\tau_c}$ Hz. The first 5 terms result in filters with a 20dB/decade attenuation, whereas Term 6 results in a 40dB/decade attenuation. Second, the presence of the $e^{-s\tau_c}$ terms in $G_{chip}(s)$ result in components of the bode diagram that are periodic with respect to $\frac{\omega\tau_c}{2\pi}$.

The influence of this filter on the gain margin of the open loop transfer function (Eq. (3)) can be readily considered. The overall stability is still dominated by the magnitude of the flexible structure's frequency response, and the cutting stiffness K_n. Furthermore, if the 'chip passing frequency', or reciprocal of the chip contact time τ_c, is much greater than the natural frequency of the flexible structure, then the influence of G_{chip} is negligible. However, if the chip passing frequency is less than the structure's natural frequency, then G_{chip} acts as filter that reduces the effective cutting stiffness. In this situation, the magnitude and phase response of G_{chip} vary over a wide range, which means that the chatter frequency and critical width of cut could also vary dramatically for some weighting functions.

It should be re-iterated that the intention here is not to perform calibration of this model (i.e. choice of weighting function and its coefficients), but rather to focus on whether this model formulation could explain observed phenomenon based upon published data regarding the approximate chip contact time τ_c. This issue will be revisited once the experimental setup has been summarised, and suitable signal processing and analysis procedures have been introduced.

3. Experimental method

In order to investigate the process damped stability of turning difficult-to-cut materials, a custom-built flexible tool holder was designed and built. The tool holder, shown in Fig. 5 involved mounting a custom turning insert (Sandvik type N123K2-0720-0002-GB prepared to give a rake angle of 7 °, relief angle 7 °) on a flexible arm. This was rigidly attached

to the turret of the CNC lathe via the standard VDI interface. The tool displacement was measured in the y direction (i.e. normal to the workpiece surface) using a Lion Precision U3B inductive sensor focussed on an aluminium target. Accelerometers were also used to measure the vibration in the y direction, and in the x direction parallel to the workpiece surface (i.e. the surface speed direction).

The flexure configuration was carefully designed so as to achieve a single-degree-of freedom behaviour in the y direction, whilst maintaining high rigidity in the x and z directions. This helped to avoid the onset of undesirable behaviour such as primary chatter or mode coupling chatter. Consequently the experimental configuration closely resembles the schematic configuration shown in Fig. 1a. The modal parameters of the flexure were measured using a modal hammer and the inductive probe, and these parameters are summarised in Table 2.

The flexible tool holder was used to machine Ti6Al4V alloy on a Cincinnati Hawk CNC lathe. The feed direction was parallel to the rotational axis of the workpiece (as shown in Fig. 5), and the workpiece was prepared such that rings of material were removed by the tool. This ensured that the side edges of the tool were not in contact with the workpiece, thus avoiding the associated rubbing forces.

For each machining test, a new ring on the workpiece surface was prepared, and a new section of tool cutting edge was used to avoid the effects of tool wear. The width of cut (i.e. the annular width of the ring on the workpiece) was maintained constant at 0.6mm, and the surface speed was varied by using different spindle speeds along with three different diameters for the workpiece ring. All cutting was performed without coolant.

The cutting stiffness K_n (Table 2) was determined by performing calibration tests using a rigid tool holder and a Kistler lathe dynamometer. The same feed rate and surface speed ranges were used as for the flexible tests. Checks were performed to ensure that the cutting stiffness did not vary significantly with chip thickness under these operating conditions, to validate the linear cutting stiffness model given by Eq. (1).

Based upon this calibrated cutting stiffness and knowledge of the flexible tool holder's modal parameters, the stability lobe diagram using the standard theory of regenerative chatter can be determined. In fact, these were the parameters that were used for the

illustrative example of Fig. 3. The limiting critical width of cut (below which chatter never occurs) is 0.15 mm. Consequently, at the low spindle speeds (< 500 rev/min) used in the machining tests chatter would be expected for all of the constant width test cuts.

3.1. Signal processing

The interpretation of vibrations during machining is a particularly challenging problem due to the measurement noise and disturbance forces that act upon the system. Measurement noise is exacerbated by the background vibration of the machine and its operating environment. The complexity of the chip removal process leads to unmodelled and non-deterministic excitation of the system. Meanwhile, the aims for this contribution are (a) to identify the presence (or otherwise) of workpiece/flank interference as illustrated in Fig. 1b; and (b) to determine the overall trends in chatter stability compared to the predictions from the 'short regenerative effect' model. Achieving these aims involves the interpretation of experimental data despite the presence of high levels of measurement noise and other behaviour. This interpretation will be performed using a combination of the Hilbert transform, histograms, and power spectral density measurements.

Considering first the issue of tool flank / workpiece interference, it can be seen from Fig. 1b that this interference can only occur when the slope of the workpiece surface exceeds that of the tool flank. This assumes a perfectly sharp tool and no elastic recovery of the just-cut surface. If the workpiece surface is sinusoidal as shown in Fig. 1b, then the maximum slope can be determined from knowledge of the vibration frequency, surface speed, and vibration amplitude. However, in practice the measured signals are plagued by non-sinusoidal behaviour, time-varying amplitude, and noise. To overcome this, the following procedure was applied:

1. The experimental data was trimmed to extract data where cutting was occurring, excluding the transient behaviour near the start and end of the cut.
2. The instantaneous surface slope was estimated based upon the numerical gradient between adjacent data points, the sampling frequency, and the workpiece surface speed.
3. The histogram of the surface gradient was plotted.

The advantage of this histogram approach compared to a root-mean-square analysis is that more information is obtained about the variation of the surface slope. For example, if flank interference starts to occur then one would expect more of the sampled slope values to lie close to the slope of the tool flank, even in the presence of measurement noise. This concept can be easily visualised on a histogram.

Meanwhile, the amplitude of the measured vibration signal is a pragmatic indicator of the 'acceptability' of a machined surface. Again, a simple averaging procedure (such as a root-mean-square method) provides less insight than a histogram approach. Consequently, the amplitude of the vibration was measured using the following procedure:

1. The experimental data was trimmed to extract data where cutting was occurring, excluding the transient behaviour near the start and end of the cut.
2. The instantaneous vibration amplitude was obtained by de-trending the vibration signal (to remove the DC component), and calculating the absolute value of the Hilbert transform of the resulting signal.
3. The histogram of the instantaneous amplitude was plotted.

This procedure can be complemented by a subjective assessment of the workpiece surface quality and the audio signals detected by the machine operator. Finally, the frequency domain vibration response was obtained using a more standard approach, namely the power spectral density via Welch's method. Taken together, these procedures allow individual test cuts to be characterised in terms of:

- Presence of tool flank/workpiece interference,
- Magnitude of vibration,
- Frequency of vibration.

In the next section, this analysis will be performed and the result compared to the stability predictions from the 'short regenerative effect' model.

4. Results

We begin by illustrating the instantaneous vibration amplitude for a sequence of experimental tests under constant feed rate and increasing surface speed. The resulting histograms are shown in Fig. 6. Here, the vibration amplitude is clearly between 5 and 10 μm for surface speeds between 10 and 20 m/min. For higher surface speeds, the vibration amplitude is lower - generally between 0 and 5 μm. Because the instantaneous amplitude is a positive value, histograms with low amplitudes become skewed. Consequently, a good general measure of vibration amplitude is the mode, not the mean, of the histogram data. These mode values are shown on Fig. 6. The mode is greater than 5 μm when the speed is less than 20 m/min. In general, modes greater than 5 μm coincided with the operator's subjective assessment of the cut as being unstable or of unacceptably poor quality. Fig. 7 shows the mode of the instantaneous vibration amplitude for all of the experimental data. It can be seen that the vast majority of cuts can be classified as stable or acceptable.

Histograms of the surface slope are shown in Fig. 8 for the same sequence of test cuts featured in Fig. 6. This is a particularly insightful result, as it demonstrates a dramatic change in the distribution of surface slope samples as the surface speed is increased. Furthermore, at speeds below 22 m/min, the extreme values of the surface slope coincide with the slope of the flank face of the tool ($\tan(7^\circ) = 0.12$). The increased frequency of occurrence near this value suggests that flank/workpiece interference has started to occur. Meanwhile, at higher surface speeds the histogram suggests a normal distribution of sampled surface slopes. The shape of these distributions can be quantified based upon the standard deviation of the data. The standard deviation is included in Fig. 8: it can be seen that values greater than 0.05 indicate the onset of flank/workpiece interference.

In Fig. 9, the dominant vibration frequency (obtained from the power spectral density of the displacement signal) is plotted versus the mode of the instantaneous vibration amplitude. Shaded markers correspond to test cuts where flank interference occurs (i.e. standard deviations greater than 0.05). Whilst this representation of the data does not show all of the process parameters, it serves to summarise the measured responses from all of the

experiments. The vast majority of test cuts possessed low amplitude vibrations that were dominated by frequencies close to the tool natural frequency. No flank/workpiece interference occured for these cuts. A small number of test cuts exhibited high amplitude dominant vibration near the natural frequency of the flexure. This is an indicator of the occurence of regenerative chatter. Two of these test cuts did not exhibit flank interference. Cross-referencing to Fig. 7 reveals that these cuts were at high surface speeds where the vibration wavelength is longer (up to 5mm) and flank/workpiece interference less likely.

The remainder of the test cuts exhibited high amplitude vibration at frequencies away from the structural resonance. This is not expected from the basic regenerative chatter theory. However, this vibration can be attributed to the chip segmentation phenomenon that frequently occurs during machining of difficult-to-cut materials. This is illustrated in Fig. 10. Here, Fig. 10a shows the power spectral density for cuts at 0.4 mm/rev and surface speed between 10 and 20 m/min. The trend in dominant frequency versus surface speed is shown in Fig. 10b. Such a relationship has been reported elsewhere in the machining literature [8]. In the context of the present study, it can be seen that high amplitude vibration at the chip segmentation frequency (or 'segmentation chatter') can occur when traditional thinking would suggest that regenerative chatter should occur.

The preceding analysis allows all of the experimental tests to be categorised as follows: stable (amplitude $< 5\mu$m), regenerative chatter (amplitude $> 5\mu$m, dominant frequency $550 - 600$Hz), flank interference (standard deviation of surface slope > 0.05), and 'segmentation chatter' (amplitude $> 5\mu$m, dominant frequency outside $550 - 600$Hz). The result is summarised in Fig. 11. It can be seen that the large majority of tests exhibited stable vibrations. At low surface speeds and higher feed rates, a number of cuts exhibited high amplitude vibrations due to the chip segmentation phenomenon, i.e. 'segmentation chatter'. In these cases, flank interference always occurred. Only 4 experimental tests exhibited high amplitude vibrations at the expected frequency for regenerative chatter. Of these, one test (0.4mm/rev, 16 m/min) involved chip segmentation frequencies in the region of the expected regenerative chatter frequency (as shown in Fig. 10b). In the remaining 3 tests, flank interference occurred once (0.7 mm/rev, 60 m/min).

Finally, the predicted stability lobes based upon the short regenerative delay model can be compared to this experimental result. It was argued in Section 2.3 that a plausible value for the chip contact time τ_c for this material is $60 \times 0.002/v_s$ seconds. The resulting bode diagram for the transfer function G_{chip} was shown in Fig. 4. Including this transfer function in the open loop transfer function, and calculating the resulting gain margin, leads to the stability lobe prediction for this model. The spindle speed for the experimental tests was always very low (< 500 rev/min), and reference to Fig. 3 indicates that the critical width of cut is effectively independent of the spindle speed under these conditions. However, the surface speed v_s varies considerably and directly influences stability through the chip contact time τ_c. Consequently the stability boundary can be plotted versus surface speed.

The resulting prediction is shown in Fig. 12 for five of the six candidate weighting functions. The result for Term 5 in Table 1 is not included for clarity, because the result was so similar to that for Terms 1 and 3. A detailed discussion of this result will follow in the next section. For now, the key finding is that for the experimental tests at 0.6mm width of cut, all of the weighting functions predict unstable behaviour for surface speeds greater than 80 m/min. Beyond here, the chip passing frequency becomes greater than the dominant vibration frequency of the tool holder, so that the short regenerative effect has little or no influence on behaviour. Consequently, this model cannot explain the experimentally observed results in Fig. 11, where 8 out of 10 tests above 80 m/min exhibited chatter free behaviour.

5. Discussion

Before drawing conclusions, a number of issues are worthy of further discussion.

The dominant frequency in many cases was between 550 and 600 Hz, compared to a natural frequency of 540Hz. Classical stability lobe theory shows that the chatter freqeuency or dominant stable frequency are slightly higher than the natural frequency of the structure, but this difference becomes very small when the spindle speed is low (as was the case here). Possible explanations for this increased dominant frequency are either an increased effective

stiffness due to the machining-induced preload of the flexible structure, or a complex chip mechanics mechanism that interacts with the regenerative effect.

Flank interference has been shown to occur for some turning tests, but only for cases where the amplitude of vibration was already quite high. This implies that the interference effect does not provide sufficient damping to stabilise chatter vibrations at an acceptable level for the experimental configuration that was used in this study. However, this may not always be the case. For example, in milling there are higher levels of forced vibration (due to tool rotation and intermittent cutting) which could induce the interference effect under cutting conditions that remain acceptable. Furthermore, different structural resonant frequencies and tool geometries would influence the workpiece surface slope. A related issue here is that the tool geometry has been considered to be completely sharp, and no elastic recovery of the just-cut material was presumed. In practice, a blunt tool tip would lead to interference at lower workpiece slopes, and any elastic recovery of the just-cut surface would have a similar effect. However, the histogram approach that was used here would be able to identify the these trends had they occurred.

The short regenerative delay model clearly has good potential in terms of explaining and predicting process damping phenomena. However, the key issue of model calibration remains unsolved, and in any case the model cannot explain all of the stability increases that were observed in this study. Nevertheless, the frequency domain solution that has been proposed here should make weighting function calibration a more feasible process. For example, the influence of different weighting functions can be observed in the stability lobe diagram, and the closed loop frequency response of the system can be readily obtained which may pave the way for alternative calibration methods. An additional advantage of this frequency domain solution is that real experimental data could be used to represent the frequency response function of the flexible structure. This is of practical value since it is common to use a modal hammer and accelerometer to capture this FRF from the actual machine/tool structure.

However, the experiments illustrated in the present manuscript have suggested that the short regenerative effect cannot provide sufficient increases in stability, regardless of the weighting function that is employed. This has been argued on the basis that other researchers

have studied tool/chip contact length in considerable detail, and this parameter directly influences the chip contact time. All of the weighting functions considered here have only improved the chatter stability when the chip contact time becomes longer than the natural period of oscillations of the flexible structure. A number of experiments produced stable behaviour even though the expected chip contact time was shorter than the natural period of oscillations of the flexible structure. Consequently this model could only emulate the experimentally observed behaviour if the chip contact time was more than twice the value obtained from the literature [15], and even then only certain forms of weighting function would provide sufficient stability increases. Admittedly there are some differences in the tool geometry and process conditions between ref. [15] and the present study, but it seems highly unlikely that this would result in a two-fold change in the chip contact time. The most likely explanation for this increased stability is the interaction of the chip segmentation phenomenon with the self-excitated vibrations, since chip segmentation is well-known for this material, and was found to dominate the vibration response in some of the tests that were performed.

6. Conclusions

This article has focussed on the low-speed turning of a difficult-to-cut titanium alloy (Ti6Al4V), and investigated the increased stability at low speeds due to the process damping phenomenon. The following specific conclusions can be drawn:

1. Flank interference is a proposed process damping mechanism that can be characterised from experimental displacement measurements by investigating the histogram of the instantaneous workpiece surface slope. This can be compared to the slope of the tool flank. Interference between workpiece and flank causes a dramatic change in the shape of the histogram that can be quantified from the standard deviation of the data. Applying this approach to the experiments in this study revealed that a number of turning experiments exhibited tool flank / workpiece interference.
2. An alternative mechanism for the process damping phenomenon (the short regenerative

effect) [9] has also been considered. A novel solution methodology has been presented that relies on a frequency domain solution. This approach allows a new interpretation of the stabilisation mechanisms behind the model, and is more amenable to solution when using experimentally obtained frequency response measurements of the flexible structure (i.e. the tool or workpiece).

3. The short regenerative effect relies on an estimation of the chip contact time on the tool rake face, along with knowledge of a weighting function that distributes the cutting force along the tool rake face as a function of the chip thickness along the rake face. This study has not aimed to validate or calibrate these model parameters, but published data has been used to obtain realistic values of the chip contact length and a wide range of potential weighting functions have been considered. It has been shown that none of these weighting functions can provide sufficient increases in stability for the model to match experimentally observed data.
4. The experimental data indicates considerably greater stability than can be explained by either the short regenerative effect or the tool flank / workpiece interference effect. Meanwhile, chip segmentation effects were commonly observed, and these could be sufficient to cause unacceptable levels of vibration amplitude. The chip segmentation effect is known to vary dramatically with surface speed and feed rate. Consequently it is suggested that the interaction between chip segmentation and self-excited vibration is likely to have a strong influence on process damped regenerative chatter for this class of materials. This aspect should be a focus of further work.

7. Acknowledgements

The authors are grateful for the support of the EPSRC through grant reference EP/D052696/1.

References

[1] J. Tlusty, Manufacturing Processes and Equipment, Prentice Hall, New Jersey, 1999.

[2] E. O. Ezugwu, Z. M. Wang, Titanium alloys and their machinability - a review, Journal of Materials Processing Technology 68 (3) (1997) 262–274.

[3] J. Tlusty, Dynamics of high-speed milling, Journal of Engineering for Industry 108 (1986) 59–67.

[4] E. Budak, L. T. Tunc, A new method for identification and modeling of process damping in machining, Journal of Manufacturing Science and Engineering 131 (5) (2009) 051019–10.

[5] M. Eynian, Y. Altintas, Chatter stability of general turning operations with process damping, Journal of Manufacturing Science and Engineering 131 (4) (2009) 041005–10.

[6] A. Yusoff, S. Turner, C. Taylor, N. Sims, The role of tool geometry in process damped milling, The International Journal of Advanced Manufacturing Technology In press.

[7] Y. Altintas, M. Weck, Chatter stability of metal cutting and grinding, CIRP Annals - Manufacturing Technology 53 (2) (2004) 619–642.

[8] S. Sun, M. Brandt, M. S. Dargusch, Characteristics of cutting forces and chip formation in machining of titanium alloys, International Journal of Machine Tools and Manufacture 49 (7-8) (2009) 561–568.

[9] G. Stepan, Retarded dynamical systems: stability and characteristic functions, Pitman Research Notes in Mathematics, Longman scientific and technical, UK, 1989.

[10] G. Stepan, Modelling nonlinear regenerative effects in metal cutting, Philosophical Transactions of the Royal Society of London, Part A 359 (2001) 739–757.

[11] Y. Altintas, Manufacturing Automation: Metal Cutting Mechanics, Machine Tool Vibrations, and CNC Design, Cambridge University Press, 2000.

[12] F. A. Khasawneh, B. P. Mann, T. Insperger, G. Stepan, Increased stability of low-speed turning through a distributed force and continuous delay model, Journal of Computational and Nonlinear Dynamics 4 (4) (2009) 041003–12.

[13] T. H. C. Childs, K. Maekawa, T. Obikawa, Y. Yamane, Metal machining : theory and applications, Arnold, 2000.

[14] S. A. Iqbal, P. T. Mativenga, M. A. Sheikh, A comparative study of the tool-chip contact length in turning of two engineering alloys for a wide range of cutting speeds, International Journal of Advanced Manufacturing Technology 42 (1-2) (2009) 30–40.

[15] S. A. Iqbal, P. T. Mativenga, M. A. Sheikh, Characterization of machining of aisi 1045 steel over a wide range of cutting speeds. part 1: Investigation of contact phenomena, Proceedings of the Institution of Mechanical Engineers, Part B: Journal of Engineering Manufacture 221 (5) (2007) 909–916.

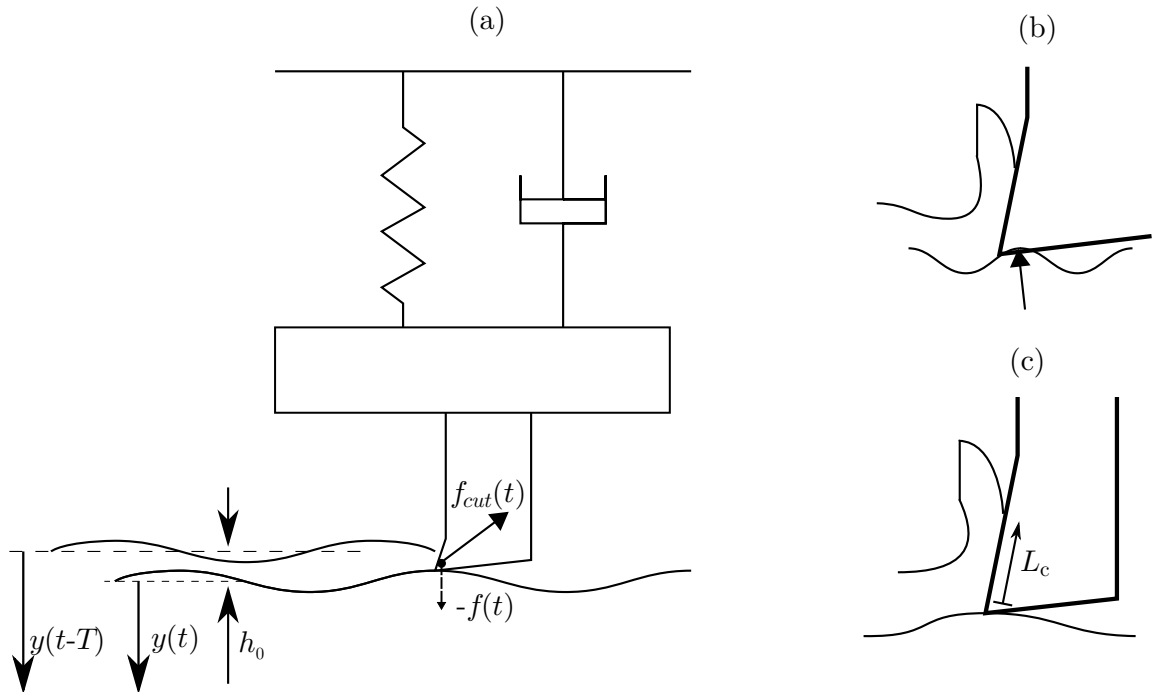

Figure 1: Schematic representation of chatter in turning. The force $-f$ is the component of f_{cut} acting in the positive y direction. (a) Regeneration of surface waviness. (b) Close up of the cutting region - the arrow indicates interference between the just-cut surface and the tool flank face. (c) Close up of the cutting region, showing length of contact L_c between tool rake face and chip.

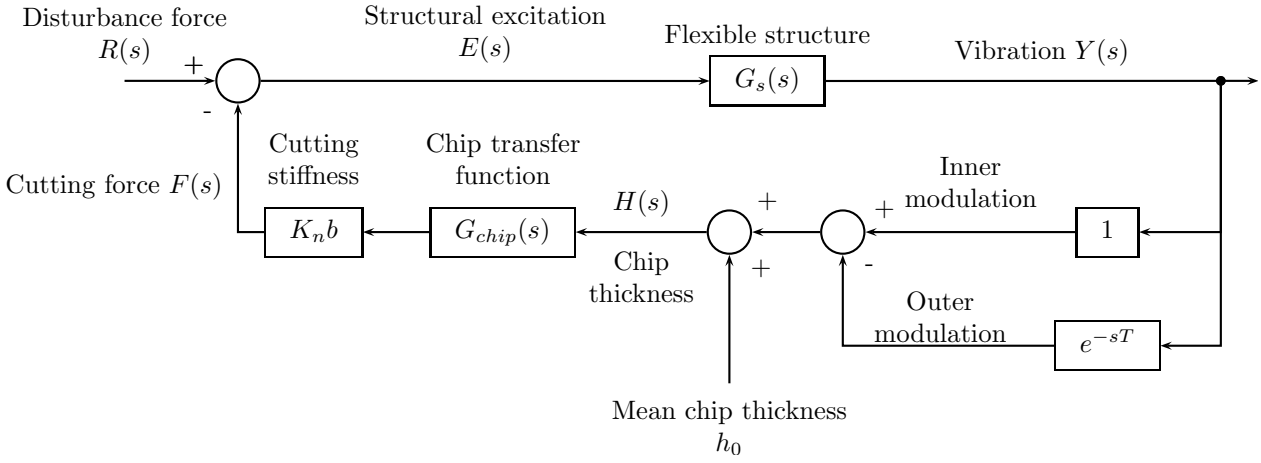

Figure 2: Block diagram of turning process. In the traditional stability model (Section 2.1), $G_{chip} = 1$

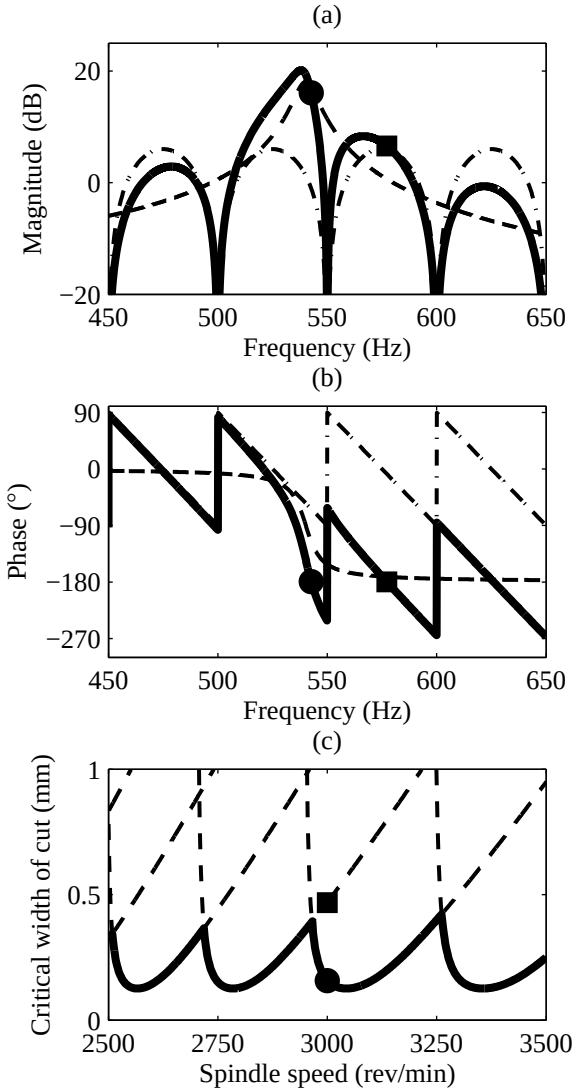

Figure 3: Open loop bode diagram and resulting chatter stability. Bode diagram magnitude (a) and phase (b) at 3000 rev/min: – – – structure and cutting stiffness ($G_s K n$); – · – regenerative delay ($1 - e^{-sT}$); ——— total. ●and ■indicate phases of -180°. Chatter stability lobes (c) with stability boundaries ●and ■from (a) and (b) shown superimposed, – – – analytical solution; ——— limiting width of cut.

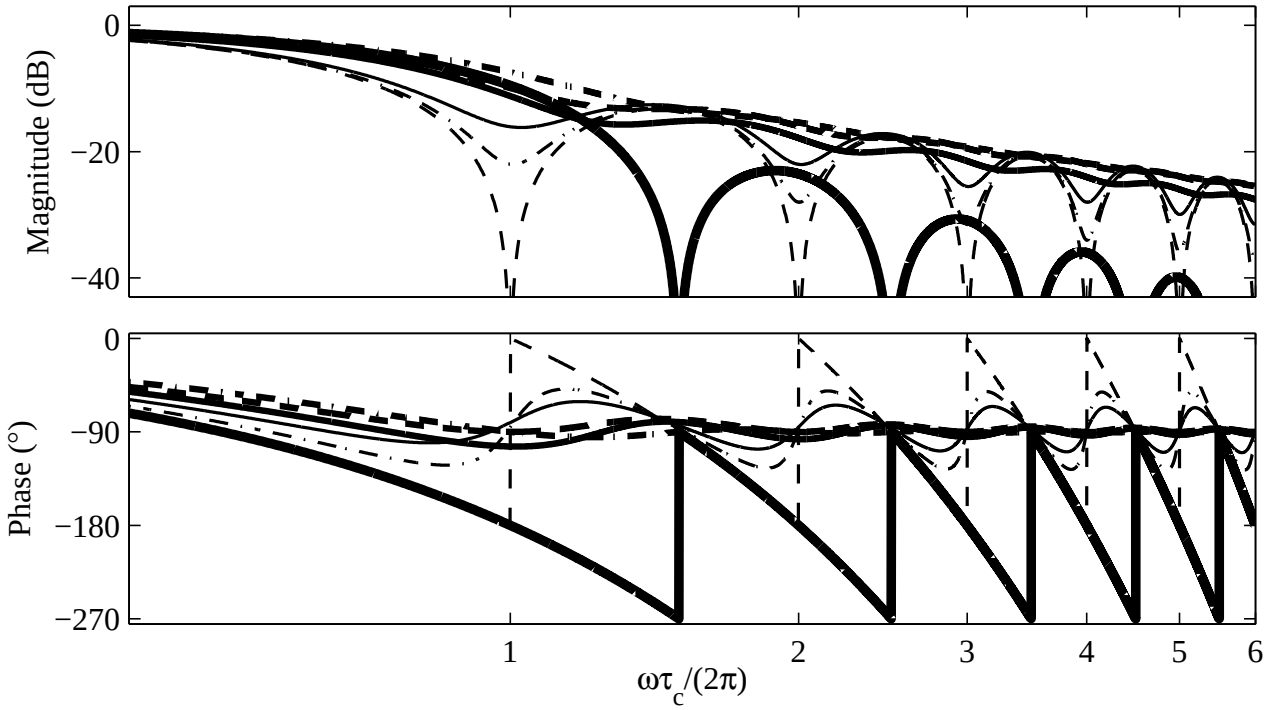

Figure 4: Bode diagram for candidate weighting functions. —— Term 1: Exponential, $a = 1$ — · — Term 1: Exponential, $a = 5$; — — — Term 2: Constant; — — — Term 3: Linear —— Term 4: Cosine — · — Term 5: Cosine+ —— Term 6: Sine;

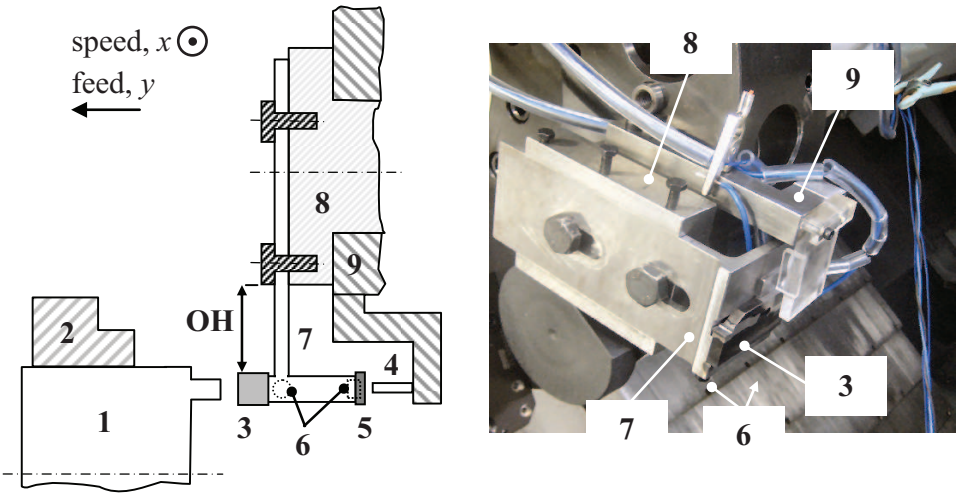

Figure 5: Experimental setup. 1 - workpiece with annular ring; 2 - lathe chuck; 3 - cutting insert in blade holder; 4 - displacement probe; 5 - aluminium target; 6 x,y accelerometers; 7 - flexure arm; 8 - base plate and VDI interface; 9 - turret and probe bracket.

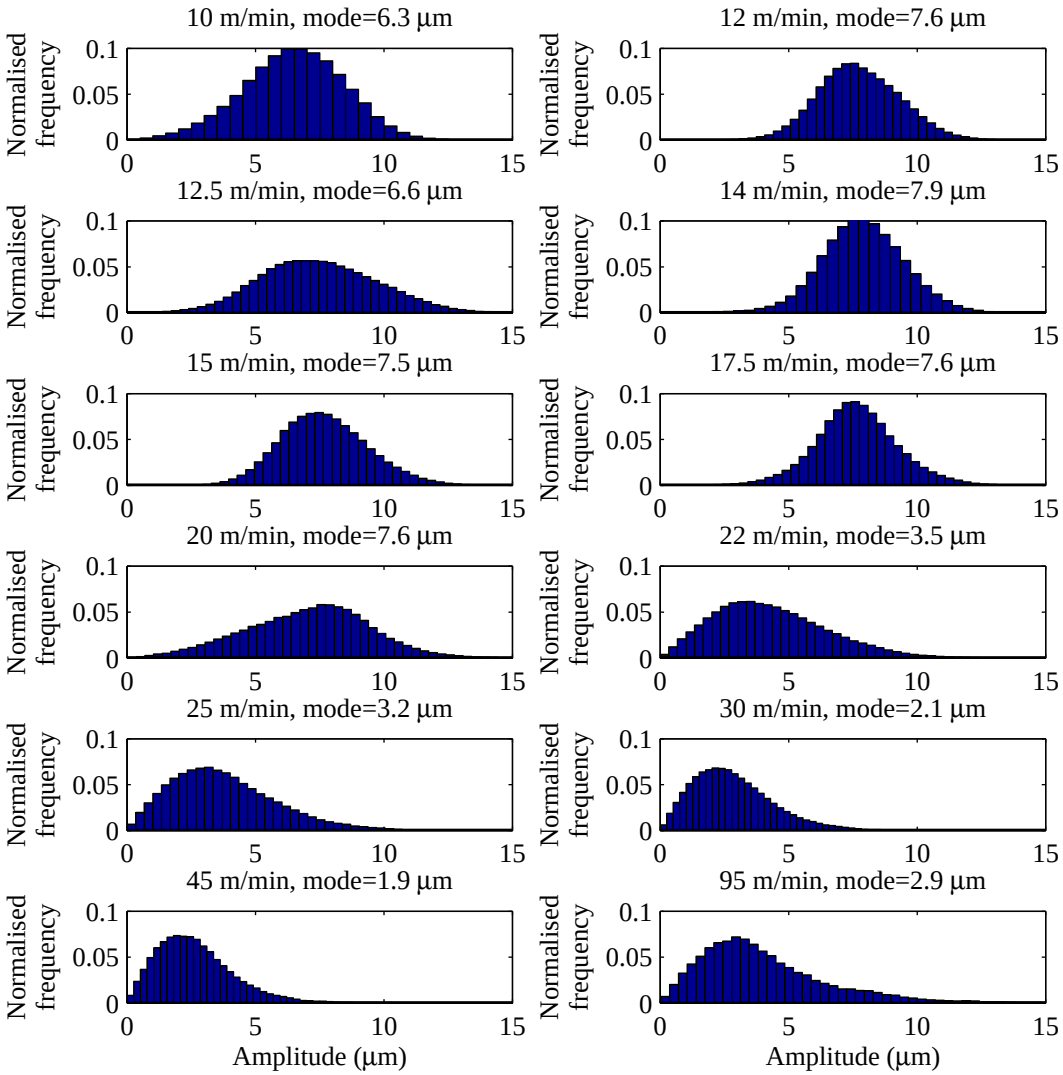

Figure 6: Histograms of the instantaneous vibration amplitude during cutting with feed rate 0.4 mm/rev and different surface speeds.

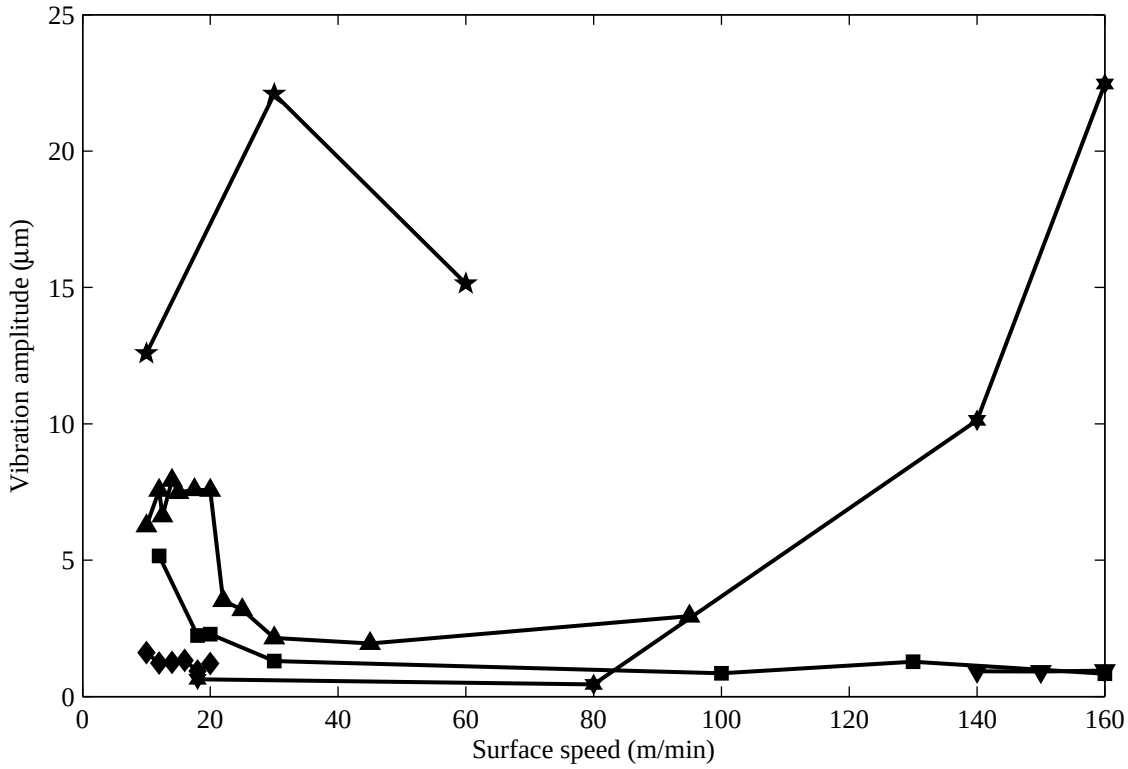

Figure 7: Vibration amplitude (i.e. mode of the histogram of the instantaneous vibration amplitude) versus surface speed. ★ 0.7 mm/rev; ▲ 0.4 mm/rev; ■ 0.3 mm/rev; ◆ 0.2 mm/rev; ▼0.15 mm/rev; ✡ 0.1 mm/rev.

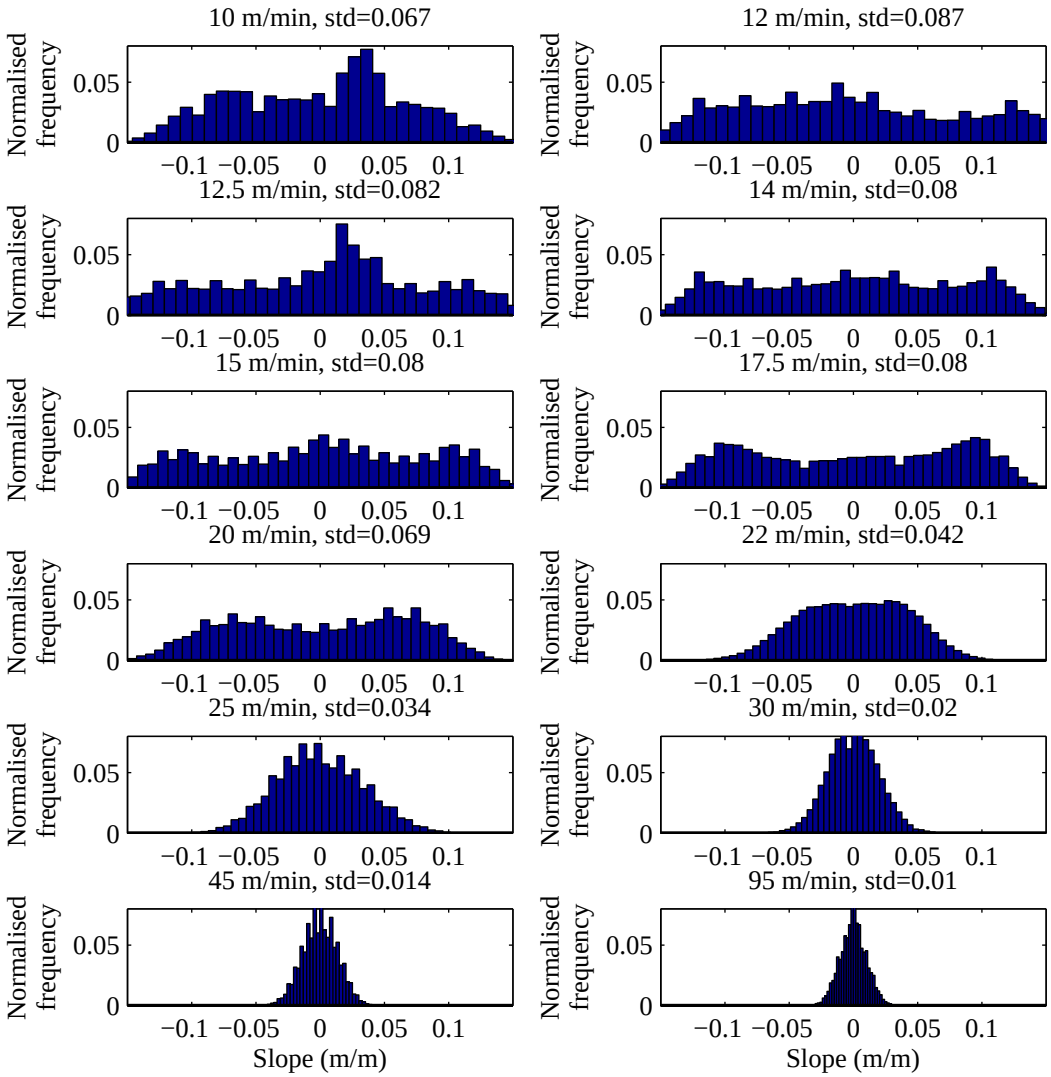

Figure 8: Histograms of the instantaneous surface slope during cutting with feed rate 0.4 mm/rev and different surface speeds. A slope of 0.122 corresponds to interference with the tool (relief angle 7°)

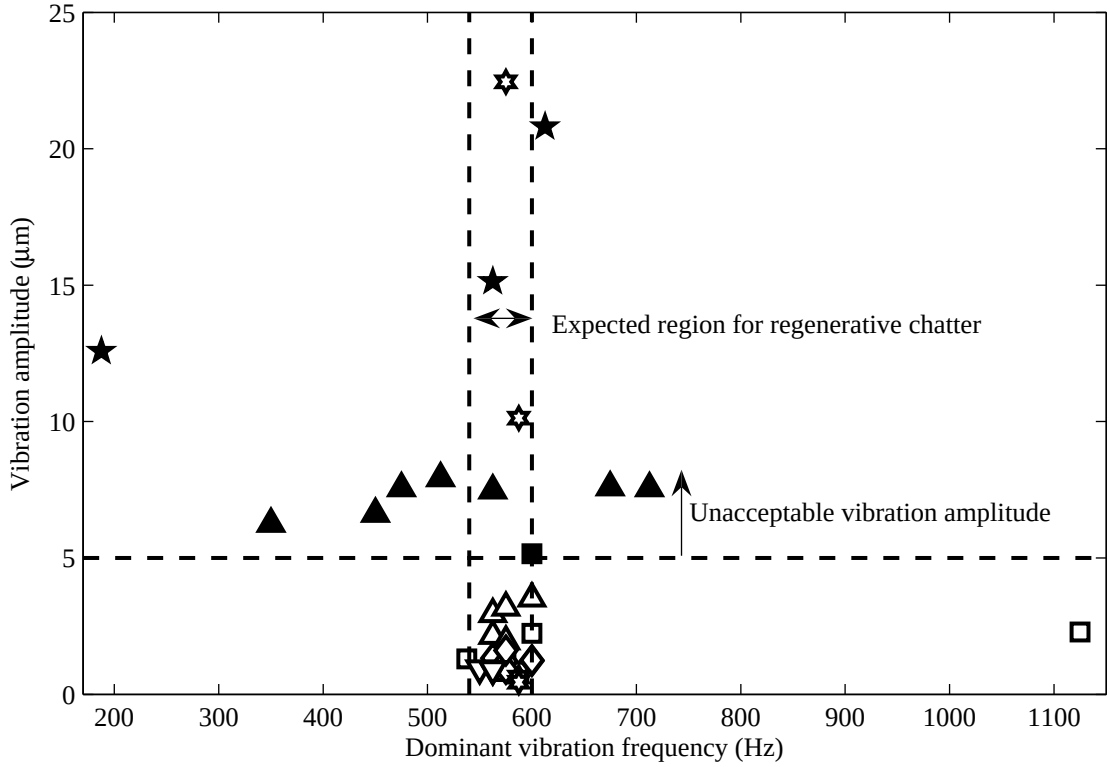

Figure 9: Vibration amplitude versus dominant vibration frequency. Filled markers indicate cuts where flank interference occurs. Marker shapes correspond to those for Fig. 7.

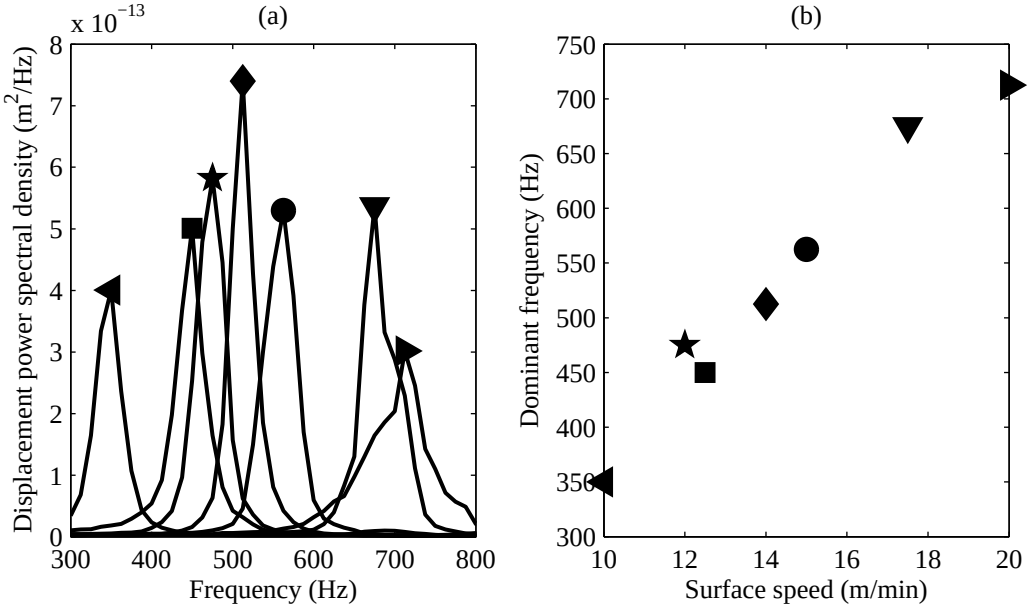

Figure 10: Power spectral density (a) and dominant frequency (b) for cuts at 0.4 mm/rev with surface speeds between 10 and 20 m/min.

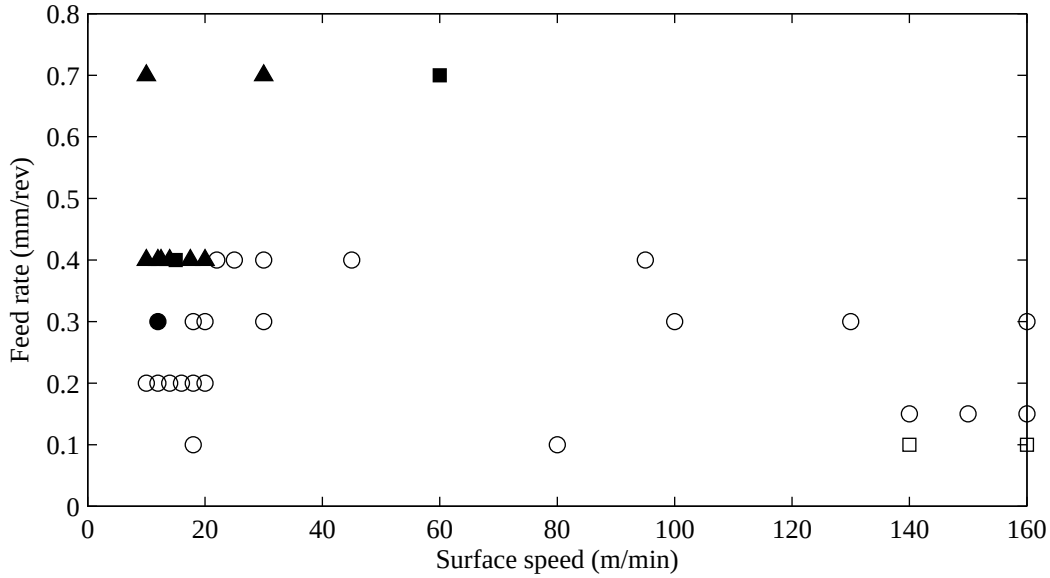

Figure 11: Summary of experimental data. Filled markers indicate cuts where flank interference occurs. Triangle markers indicate Segmentation chatter; Square markers indicate regenerative chatter; Circular markers indicate no chatter.

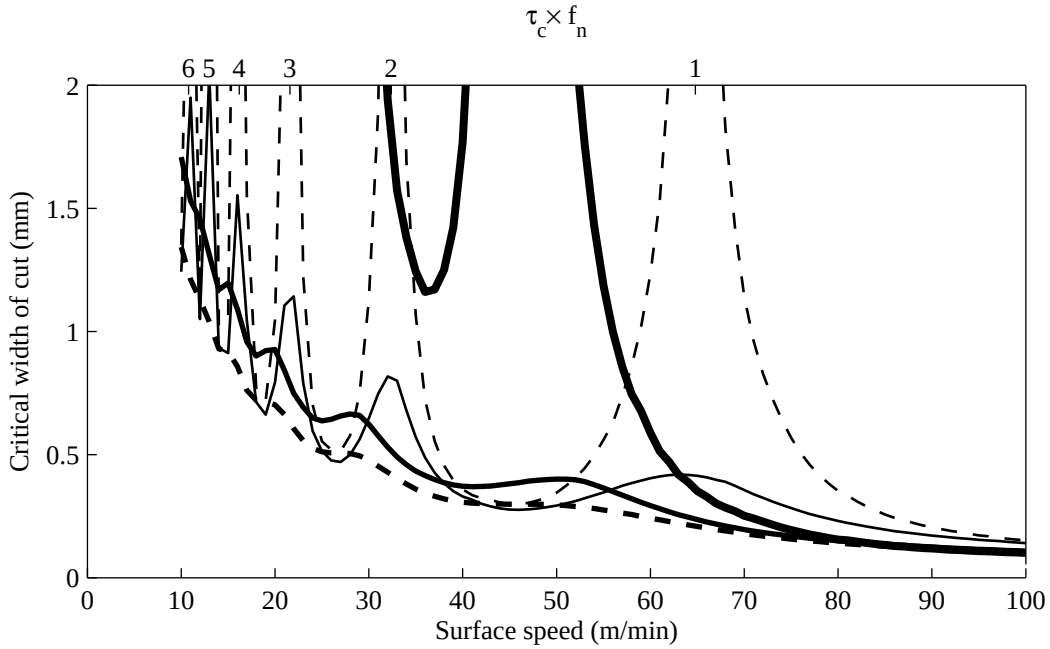

Figure 12: Influence of weighting functions on chatter stability. $\tau_c = 0.01 \times 60/v_s$. The top axis indicates situations where the chip passing frequency (in Hz) is a multiple of the structure's natural frequency (in Hz). — · — Term 1: Exponential, τ_c =; — — — Term 2: Constant; — — — Term 3: Linear, ——— Term 4: Cosine; ——— Term 6: Sine

Description	$w(\tau)$	$G_{chip}(s)$
1. Exponential	$\frac{a}{\tau_c(1-e^{-a})} e^{\frac{-a\tau}{\tau_c}}$	$\left(\frac{a}{e^a-1}\right)\left(\frac{1}{a+s\tau_c}\right)(e^a - e^{-s\tau_c})$
2. Constant	$\frac{1}{\tau_c}$	$\frac{1-e^{-s\tau_c}}{s\tau_c}$
3. Linear	$\frac{2}{\tau_c}\left(1-\frac{\tau}{\tau_c}\right)$	$\frac{2\left(s\tau_c - 1 + e^{-s\tau_c}\right)}{\tau_c^2 s^2}$
4. Cosine	$\frac{\pi\cos\left(\frac{\pi\tau}{2\tau_c}\right)}{2\tau_c}$	$\frac{\pi\left(2s\tau_c + \pi e^{-s\tau_c}\right)}{4s^2\tau_c^2 + \pi^2}$
5. Cosine+	$\frac{1+\cos\left(\pi\tau/\tau_c\right)}{\tau_c}$	$\frac{2s^2\tau_c^2 + \pi^2 - e^{-s\tau_c}\pi^2}{\tau_c s\left(s^2\tau_c^2 + \pi^2\right)}$
6. Sine	$-\frac{pi}{2\tau_c}\sin\left(\frac{\pi\tau}{\tau_c}\right)$	$\frac{\pi^2\left(\mathrm{e}^{s\tau_c}+1\right)\mathrm{e}^{-s\tau_c}}{2\left(s^2{\tau_c}^2 + \pi^2\right)}$

Table 1: Selected weighting functions and the resulting chip transfer functions. Terms 1 ($a = 1$), 5, and 6 were proposed by [9].

Parameter	Value
Natural frequency f_n (Hz)	540.2
Damping ratio (-)	0.0096
Effective stiffness (kN/mm)	4.314
Cutting stiffness K_n (N/mm^2)	667

Table 2: Modal parameters of the flexible tool holder, and cutting stiffness of the workpiece/tool.